Dijlah Journal of Engineering Science (DJES) Vol. 3, No. 2, June, 2026, pp. 222-232
ISSN: Printed: **3078-9656, Online: 3078-9664**, paper ID: 161

Multiaxial Stress States and Failure Evolution in Laminated Structural Plates under Contact Loading

Ali Qasim Abdulwahid
Basra University, Department of Mechanical Engineering

Article Info

Article history:

Received Jan, 27, 2026
Revised Feb.,9, 2026
Accepted Mar.,4, 2026

Keywords:

Multiaxial stress
Dynamic loading
FEA
Deformation
Fatigue and damage

Abstract

Mechanical structures operating under real service conditions are frequently subjected to variable dynamic loads that generate complex multiaxial stress states and time-dependent deformation behaviour. Accurate prediction of stress distribution and structural response under such conditions is essential to ensure safety, reliability, and long-term performance. This study presents a comprehensive multiaxial stress and deformation analysis of mechanical structures subjected to variable dynamic loading, with emphasis on the combined effects of normal, shear, and cyclic stresses. The analysis is conducted using advanced finite element modelling techniques, where realistic loading scenarios are applied to simulate operational conditions. Material nonlinearities, geometric effects, and dynamic load variations are incorporated to capture the true mechanical response of the structure. Stress components are evaluated in multiple directions, and equivalent stress criteria such as von Mises and principal stress theories are employed to assess failure risks. Additionally, deformation behaviour, strain localization, and stress concentration regions are examined to identify critical zones susceptible to fatigue and structural degradation. The results demonstrate that multiaxial loading significantly influences stress interaction and deformation patterns, leading to higher stress amplitudes and non-uniform strain distribution compared to uniaxial loading assumptions. Dynamic load variations are shown to amplify localized stresses and accelerate damage initiation, particularly in regions with geometric discontinuities. The findings highlight the necessity of multiaxial analysis in mechanical design and provide valuable insights for improving structural optimization, fatigue life prediction, and damage prevention strategies. This study contributes to a more realistic assessment of mechanical structural behavior under dynamic service conditions and supports the development of safer and more efficient engineering designs.

Corresponding Author:

Ali Qasim Abdulwahid
Basra University, Department of Mechanical Engineering
Email: pmssupervisoridc@gmail.com

1. Introduction

The increasing use of advanced mechanical structures in highly demanding engineering applications, such as aerospace, energy, and industrial systems, necessitates a detailed understanding of their behavior under variable dynamic loading conditions. These structures are often exposed to complex multiaxial stress states resulting from combined normal, shear, and out-of-plane loads, which significantly influence deformation patterns, damage initiation, and failure evolution. While many materials and structural configurations exhibit enhanced strength and stiffness, their response under dynamic and non-proportional loading remains a critical design challenge.

One of the main limitations in evaluating structural integrity under dynamic loads lies in the difficulty of experimentally characterizing damage mechanisms due to the short duration, high strain rates, and increased dispersion of results. Consequently, quasi-static testing approaches have frequently been employed as simplified alternatives to dynamic loading scenarios. However, the extent to which quasi-static results can reliably represent structural behavior under dynamic conditions remains an open question, particularly in the presence of multiaxial stress and deformation interactions. This study addresses this gap by performing a detailed multiaxial stress and strain analysis of mechanical structures subjected to variable loading rates. Special attention is given to the role of material anisotropy and directional deformation, investigated through full-field strain measurements obtained using Digital Image Correlation (DIC) and supported by Finite Element Method (FEM) simulations. The combined experimental– numerical approach enables the evaluation of stress interaction effects, deformation localization, and critical damage thresholds. Furthermore, the study examines similarities and differences in structural response under different loading regimes by correlating force–displacement behavior and energy absorption characteristics. The results demonstrate that key stages of damage initiation and evolution can be identified based on multiaxial stress states, showing partial independence from strain rate effects up to final failure. These findings contribute to a more unified framework for predicting deformation and failure in mechanical structures under variable dynamic loads, supporting improved design, assessment, and reliability of engineering components.

2. Experimental and numerical procedure.

The mechanical structures investigated in this study are manufactured using laminated composite configurations representative of advanced engineering materials commonly employed in high-performance applications. The specimens are produced from unidirectional prepreg plies with a toughened polymeric matrix reinforced by high-strength carbon fibres, ensuring high stiffness-to-weight ratio and pronounced anisotropic behavior. The laminates are fabricated through a controlled hand lay-up process following a predefined stacking sequence, after which a curing cycle recommended by the material supplier is applied using a hot platen press to ensure consistent consolidation and material quality. After curing, the laminates are machined into square plate specimens with nominal side dimensions of 80mm. The average cured ply thickness is approximately 0.25 mm, resulting in a laminate thickness representative of thin structural components subjected to bending and out-of-plane loading. The elastic properties of the lamina in the principal material directions, including elastic moduli, shear moduli, and Poisson's ratios, are adopted from validated experimental data available in the literature and are used as input parameters for the numerical simulations.To investigate the structural response under different loading rates, two complementary testing methodologies are employed: quasi-static indentation (QSI) and low-velocity impact (LVI). For both procedures, identical specimen geometries and boundary conditions are applied to allow direct comparison of the multiaxial stress and deformation states. The specimens are simply supported on a circular fixture with a span diameter of 74 mm, while a hemispherical indenter with a radius of 10 mm applies a concentrated load at the centre of the plate.In the quasi-static indentation tests, displacement-controlled loading is applied at a constant rate of 0.8 mm/s using an electromechanical testing machine. Full-field surface deformation and strain distributions on the upper face of the specimen are measured using a three-dimensional Digital Image Correlation (DIC) system, enabling detailed analysis of radial and tangential strain components. Simultaneously, local strain measurements at the centre of the bottom surface are recorded using a triaxial strain gauge rosette, allowing accurate evaluation of the multiaxial strain state induced by bending and indentation. The combined experimental approach provides comprehensive insight into stress interaction, deformation localization, and damage initiation under variable loading conditions. The resulting data serve as a basis for correlating quasi-static and dynamic responses and for validating finite element models aimed at predicting multiaxial stress and deformation behavior in mechanical structures subjected to variable dynamic loads.

To investigate the structural response under different loading rates, two complementary testing methodologies are employed: quasi-static indentation (QSI) and low-velocity impact (LVI). For both procedures, identical specimen geometries and boundary conditions are applied to allow direct comparison of the multiaxial stress and deformation states. The specimens are simply supported on a circular fixture with a span diameter of 74 mm, while a hemispherical indenter with a radius of 10 mm applies a concentrated load at the centre of the plate. To investigate the structural response under different loading rates, two complementary testing methodologies are employed: quasi-static indentation (QSI) and low-velocity impact (LVI). For both procedures, identical specimen geometries and boundary conditions are applied to allow direct comparison of the multiaxial stress and deformation states. The specimens are simply supported on a circular fixture with a span diameter of 74 mm, while a hemispherical indenter with a radius of 10 mm applies a concentrated load at the centre of the plate. In the quasi-static indentation tests, displacement-controlled loading is applied at a constant rate of 0.8 mm/s using an electromechanical testing machine. Full-field surface deformation and strain distributions on the upper face of the specimen are measured using a three-dimensional Digital Image Correlation (DIC) system, enabling detailed analysis of radial and tangential strain components. Simultaneously, local strain measurements at the centre of the bottom surface are recorded using a triaxial strain gauge rosette, allowing accurate evaluation of the multiaxial strain state induced by bending and indentation. The combined experimental approach provides comprehensive insight into stress interaction, deformation localization, and damage initiation under variable loading conditions. The resulting data serve as a basis for correlating quasi-static and dynamic responses and for validating finite element models aimed at predicting multiaxial stress and deformation behavior in mechanical structures subjected to variable dynamic loads.

Table 1; Elastic properties of the laminated material in principal directions

Property	Description	Value
E_1 (GPa)	Longitudinal elastic modulus (fiber direction)	177.56
E_2 (GPa)	Transverse elastic modulus	11.84
E_3 (GPa)	Through-thickness elastic modulus	11.84
G_{12} (GPa)	In-plane shear modulus	5.42
G_{13} (GPa)	Longitudinal–thickness shear modulus	5.42
G_{23} (GPa)	Transverse–thickness shear modulus	3.10
ν_{12} (–)	Poisson's ratio (1–2)	0.39
ν_{13} (–)	Poisson's ratio (1–3)	0.39
ν_{23} (–)	Poisson's ratio (2–3)	0.36

The elastic properties presented in Table 1 provide a fundamental basis for understanding the multiaxial stress and deformation response of laminated mechanical structures subjected to variable dynamic loads. These properties clearly demonstrate the strongly anisotropic and orthotropic nature of the material system, which is a defining characteristic of laminated composite structures and a critical factor governing their mechanical behavior under both quasi-static and dynamic loading conditions. One of the most prominent features of the elastic response is the pronounced difference between the longitudinal elastic modulus E1 and the transverse moduli E2 and E3 The longitudinal modulus reaches a value of 177.56 GPa, which is more than an order of magnitude higher than the transverse and through-thickness moduli, both equal to 11.84 GPa. This disparity highlights the dominant load-carrying role of the reinforcing fibers along their principal direction. In mechanical structures subjected to multiaxial loading, such stiffness contrast leads to highly non-uniform stress redistribution, particularly when loads are applied out of plane or in directions misaligned with the fiber orientation. Under bending-dominated conditions, such as those induced by indentation or impact loading, the high value of E 1results in strong resistance to deformation along the fiber direction, while the comparatively low transverse stiffness allows greater deformation and strain localization across the laminate thickness. This effect becomes particularly critical in angle-ply or quasi-isotropic stacking sequences, where stress components are redistributed among plies with different orientations, leading to complex multiaxial stress states that cannot be captured using isotropic assumptions

The shear moduli values further emphasize the anisotropic mechanical response of the laminate. The in- plane shear modulus G12 and the longitudinal–thickness shear modulus G13 exhibit identical values of 5.42 GPa, whereas the transverse–thickness shear modulus G23 is significantly lower at 3.10 GPa. This reduction in G23 indicates a lower resistance to shear deformation involving the through-thickness direction, which plays a crucial role in damage initiation mechanisms such as matrix cracking and interlaminar delamination. In the context of multiaxial stress analysis, shear stresses often act as coupling components between normal stresses, particularly under non-proportional loading or dynamic excitation. The relatively low value of G23 facilitates the development of out-of-plane shear strains when the structure is subjected to localized contact forces or dynamic impacts. This behavior is strongly associated with the initiation of delamination at ply interfaces, especially in regions experiencing high bending curvature and stress concentration. The Poisson's ratios listed in Table 1 also provide important insight into the deformation coupling mechanisms inherent to the laminate. The relatively high values of ν12 and ν13 both equal to 0.39, indicate significant lateral contraction or expansion when the material is loaded along the fiber direction. This coupling effect contributes to the redistribution of stresses across different material directions, particularly under multiaxial loading scenarios where normal and shear stresses coexist. The Poisson's ratio ν23 with a value of 0.36, further highlights the coupling between transverse and through-thickness deformation. In bending and indentation problems, this coupling can lead to amplified transverse strains and increased susceptibility to matrix-dominated failure modes. Such deformation interactions are especially relevant in dynamic loading cases, where inertia effects and strain rate sensitivity may amplify local stress and strain responses. From a multiaxial stress perspective, the elastic constants summarized in Table 1 define the stiffness matrix governing the stress–strain relationships in the material's principal coordinate system. When transformed into the global coordinate system of the structure, particularly in laminates with angle-ply configurations, these properties give rise to complex stress interaction patterns. Normal stresses along one direction may induce shear strains in another, while through-thickness stresses interact with in-plane deformation, resulting in a fully coupled multiaxial response. The implications of these elastic properties become even more pronounced under variable dynamic loading. Dynamic loads introduce time-dependent stress components, inertia effects, and potential resonance phenomena, all of which interact with the inherent anisotropy of the material. The high longitudinal stiffness contributes to efficient load transmission along fiber directions, while the lower transverse and shear stiffnesses govern energy absorption, deformation localization, and damage evolution. Consequently, the laminate may exhibit significantly different responses under quasi-static and dynamic conditions, despite similar global force–displacement behavior. In experimental investigations such as quasi-static indentation and low-velocity impact tests, these elastic properties directly influence the observed force–displacement curves and strain field distributions. The early stages of loading are typically dominated by elastic bending behavior, where stiffness is primarily controlled by E1 As loading progresses, transverse and through-thickness deformation become increasingly significant, activating stress components governed by E2, and G23 . This transition often coincides with the onset of damage mechanisms such as matrix cracking and delamination. Moreover, the elastic anisotropy captured in Table 1 explains why similar damage mechanisms may appear under both quasi-static and dynamic loading conditions, even though the strain rates differ significantly. The fundamental stress–strain relationships remain governed by the same stiffness parameters, allowing certain critical stress and energy thresholds to be identified independently of loading rate, up to the point where rate-dependent material behavior becomes dominant. From a numerical modeling standpoint, accurate representation of the elastic constants in Table 1 is essential for reliable finite element simulations. These properties serve as primary inputs for predicting multiaxial stress distributions, deformation patterns, and failure initiation under variable dynamic loads. Any simplification or isotropic approximation would lead to significant errors in stress prediction, particularly in regions experiencing combined bending, shear, and contact loading. In summary, the elastic properties presented in Table 1 play a central role in defining the multiaxial stress and deformation behavior of laminated mechanical structures. The strong anisotropy, characterized by high longitudinal stiffness, reduced transverse and shear stiffness, and significant deformation coupling through Poisson's ratios, governs stress interaction, deformation localization, and damage evolution under variable dynamic loading conditions. Understanding and accurately incorporating these properties is therefore indispensable for the design, analysis, and reliability assessment of advanced mechanical structures subjected to complex service environments.

3. Results and discussion

This section describes the experimental results obtained in the QSI and LVI tests, analyzing the similarities in the recorded data and detailing the failure modes observed in the fractographies for the tested specimens. Furthermore, the analysis of the multidirectional strain state is completed with the comparison of the normal strain contours obtained by DIC and FEM.

3.1. Experimental results

The results obtained for two groups of [±45]4S specimens respectively tested under QSI and LVI are detailed below. The force-displacement and energy-displacement curves obtained for two representative tests are shown in Figure 1, although note that this study collects the numerical data from a campaign of repetitive tests. Figure 3a depicts a significant difference in the apparent stiffness of the laminate, leading to an average rigidity that is 36.3% higher in the case of LVI.

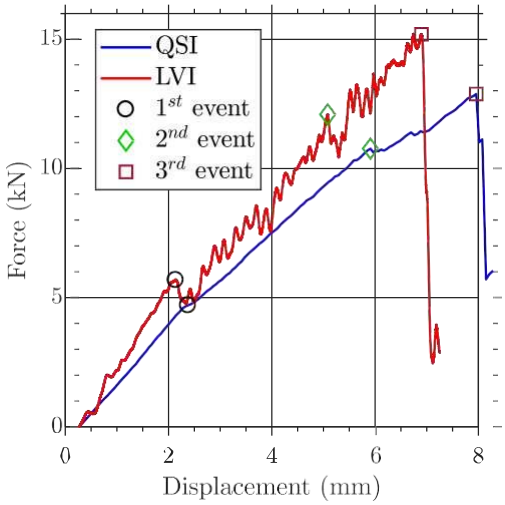

Figure 3. Representative curves for the [±45]4S under QSI and LVI, featuring the most notable events: (a) Force-deflection n terms of force or displacement However, when the dynamic oscillatory component inherent to the LVI response is disregarded, a clear qualitative similarity between the force–displacement curves obtained from quasi-static indentation and low-velocity impact tests can be observed. Both loading conditions exhibit distinct transition points along their respective evolutions, indicating comparable changes in structural behaviour and suggesting the activation of similar damage mechanisms. This observation supports the hypothesis that, despite differences in loading rate, the underlying failure processes follow analogous paths. A more quantitative comparison can be achieved by analysing the critical events identified in **Figure 1** in terms of internal energy. The internal energy, calculated as the area under the force–displacement curve, provides a physically meaningful parameter for correlating structural response under different loading regimes. As illustrated in **Figure 1**, the internal energy associated with the three characteristic events differs by only 6.5%, 3.0%, and 1.8%, respectively, when comparing quasi-static and impact tests, based on average values. These relatively small discrepancies indicate a strong correlation between both testing methodologies, reinforcing the notion that the initiation and progression of damage phenomena are primarily governed by energy thresholds rather than by the applied loading rate.The close agreement in internal energy levels at corresponding events allows for the identification of a consistent relationship between the onset and evolution of dominant damage mechanisms, particularly the formation and growth of macrocracks. This behaviour appears to be largely independent of the deformation rate within the range of velocities considered, highlighting the suitability of quasi-static tests as a representative tool for assessing certain aspects of impact-induced damage in laminated structures. This interpretation is further supported by post-test optical inspections of the specimens. Visual examination of the damaged plates provides valuable insight into the spatial distribution and nature of the failure mechanisms. **Figure 1** presents photographs of both the upper (loaded) and lower faces of a representative specimen subjected to variable loading conditions. When specimens tested under quasi-static indentation are inspected at comparable internal energy levels, very similar damage patterns are observed, confirming the consistency of the energy-based correlation.

Considering that the plate is subjected to bending in all radial directions during indentation or impact, tensile stresses and strains are expected to develop on the bottom surface across all radial orientations. These tensile components reach their maximum magnitude at the mid-span of the specimen, where the bending moment is also at its highest. Consequently, the bottom surface becomes a critical region for the initiation of tensile-driven damage mechanisms. In addition to bending-induced normal stresses, significant out-of-plane shear stresses and strains are generated, reaching maximum values near the neutral fibre of the laminate, which coincides with the midplane when tensile and compressive responses are approximately symmetric. Furthermore, pronounced stress and strain concentrations arise in the vicinity of the indenter–specimen contact region. These localized effects promote early damage initiation in the upper layers of the laminate, where compressive stresses dominate. As shown in **Figure 1**, a clear indentation imprint is observed at the centre of the plate, evidencing localized deformation and matrix-dominated damage. The coexistence of bending-induced tensile stresses, through-thickness shear, and contact-induced stress concentrations results in a complex multiaxial stress state, which governs the sequence and interaction of failure mechanisms under both quasi-static and dynamic loading conditions.

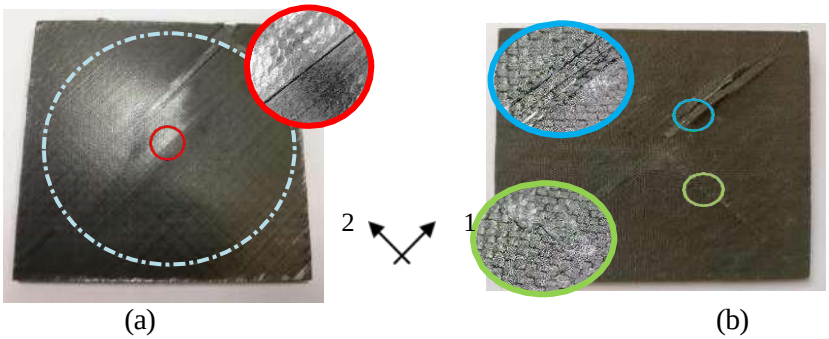

Figure *2*. Failure modes of the angle-ply laminate under LVI. (a) Bottom/tensile face view. (b) Upper/compressed face. The fibre orientation at the outer ply is symbolised with the material principal directions.

A detailed examination of the most highly tensioned surface confirms that the central region of the plate is subjected to the maximum normal tensile stresses as a direct consequence of bending-dominated loading. This region experiences the highest bending moment, leading to elevated tensile strains across all radial directions. At the ply level, the highest elastic stiffness is aligned with the fibre direction, which in this configuration corresponds to an orientation of 45°. As a result, fibre–matrix debonding is identified as the earliest damage mechanism, since the fibre–matrix interface represents the weakest link when exposed to multiaxial tensile stress states. The initiation of microcracks at the fibre–matrix interface promotes the development of larger matrix cracks that propagate preferentially along the diagonal direction. The intensity of these cracks is greatest in the central zone, where stress levels are highest, and gradually decreases as the cracks extend away from this region due to the reduction in bending moment. The formation of large matrix cracks marks the onset of significant damage and corresponds to the first characteristic transition observed in the mechanical response. Although initially localized, this damage extends into the internal plies, with crack orientation alternating according to the fibre direction of each ply. As the damage approaches the laminate mid-plane, the crack length diminishes, reflecting the lower stress levels near the neutral fibre. In parallel with matrix cracking, interlaminar delamination develops between adjacent plies as a consequence of the combined action of bending-induced normal stresses and out-of-plane shear stresses. The growth of delaminated regions contributes substantially to the progressive loss of structural stiffness and is associated with internal energy dissipation during loading. This interaction between matrix cracking and delamination governs the gradual degradation of the structural response following damage initiation. On the surface subjected to compressive loading, the failure mechanisms exhibit a more complex nature. While matrix-dominated cracking remains the primary mode due to the comparatively lower compressive strength of the polymer matrix, localized fibre kinking may also occur in regions experiencing high compressive stresses beneath the loading point. These fibre instability phenomena indicate the activation of additional damage mechanisms as deformation increases.

Despite the presence of fibre kinking, matrix cracking continues to dominate the damage evolution. Large cracks propagate along the diagonal direction, again driven by fibre–matrix debonding, and extend towards the supported boundaries of the plate. This stage corresponds to a significant increase in damage extent and marks a second transition in the mechanical response, characterized by a noticeable reduction in stiffness and an acceleration of damage propagation. The final stage of failure is strongly influenced by out-of-plane shear stresses, which become dominant as deformation progresses. These stresses facilitate unstable damage growth through the thickness of the laminate, leading to a pronounced loss of load-carrying capacity and an abrupt opening near the laminate mid-plane. The resulting failure reflects the combined effect of bending, shear, and contact-induced stress concentrations, producing a highly multiaxial stress state that ultimately governs the collapse of the structure.

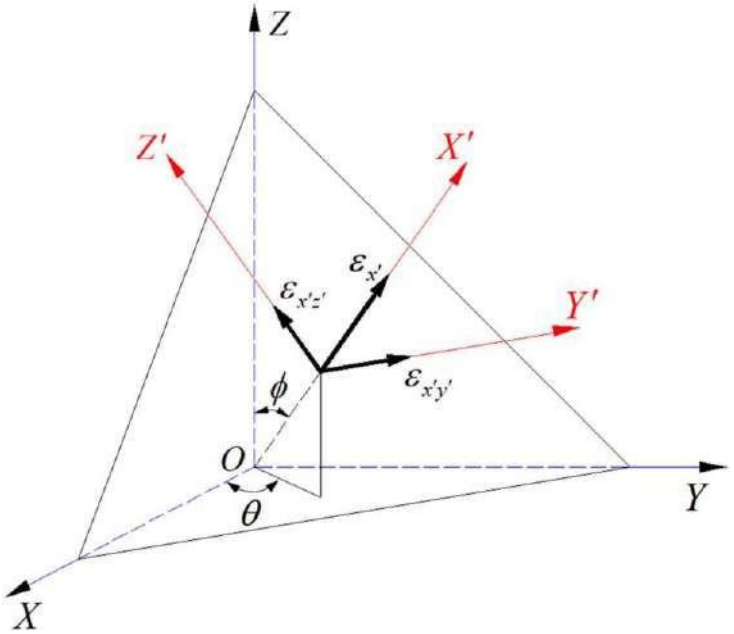

Figure 3. Generic material plane Δ and definition of angles Φ and θ.

1.1.1. Plane Stress State

For a thin-walled tubular component experiencing complicated axial–torsional load- ings as depicted within Figure 6a, the investigative material planes are all orthogonal to the specimen surface, as shown within Figure 6b. In such a case, the applied strains and stresses are able to be denoted as Equations (19) and (20):

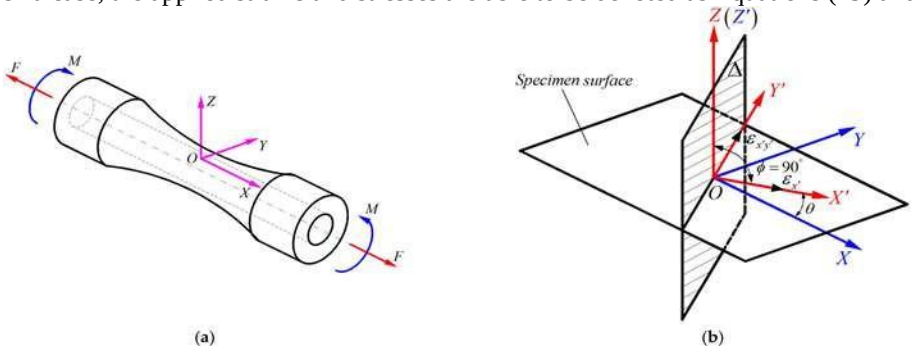

Figure 4. (a) Thin-walled tubular specimen subjected to combined tension and torsion loading; and (b) Material plane Δ perpendicular to component surface and having normal vector X′ at angle θ to X-axis.

1.2. Multiaxial Cycle Count Method

With regard to multiaxial variable amplitude load, an appropriate cycle count method is needed to enumerate numerous separate cycles within a load sequence. According to the equivalent von Mises strain rule and rain-flow count method, Wang and Brown suggested a multiaxial reversal count method The equivalent von Mises strain can be computed utilizing the algorithm as follows:

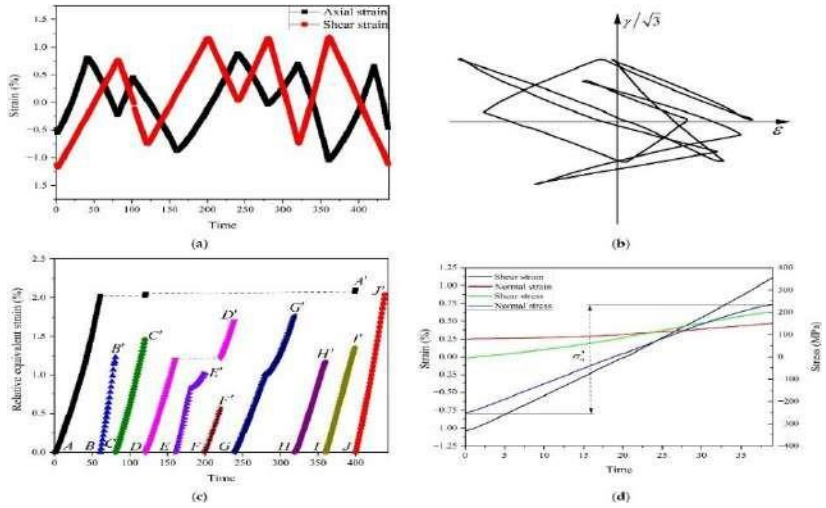

Figure 5. (a) Strain-time variable amplitude axial and torsional loading histories, (b) strain loading paths $\gamma/3 - \varepsilon$ strain space, (c) equivalent relative strain histories counted

Constrained by indenter, supports and load application system, only half of the top surface can be measured.

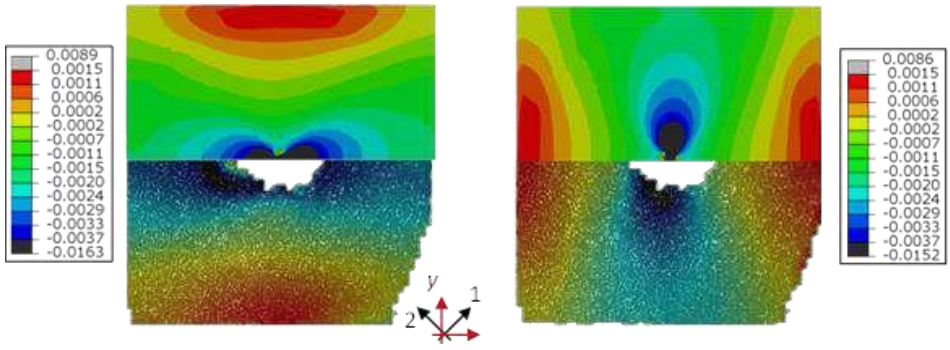

Figure 6. Comparison of experimental (top) and numerical (bottom) strain fields at uppermost Compressed ply: (a) ε_{xx} and (b) ε_{yy}. Local coordinate system for the observed ply is included.

The similarities between both approaches are clearly evident in terms of numerical values and the overall distribution patterns of the strain fields. The strain response exhibits a noticeable lack of symmetry with respect to the orthogonal directions, which can be attributed to the flexural orthotropy of the laminate. In particular, the [±45]4Slaminate demonstrates a significant directional dependence of flexural stiffness when evaluated along the material principal axes. The maximum apparent flexural stiffness develops along the direction aligned with the fibres of the outermost ply, leading to an anisotropic bending response.

Table 2; Experimental Testing Parameters under Quasi-Static and Dynamic Loading

Parameter	Quasi-Static Indentation (QSI)	Low-Velocity Impact (LVI)
Loading type	Displacement-controlled	Energy-controlled
Loading rate	0.8 mm/s	Variable impact velocity
Indenter geometry	Hemispherical	Hemispherical
Indenter radius (mm)	10	10
Support span diameter (mm)	74	74
Boundary condition	Simply supported	Simply supported

Table 2. summarizes the experimental conditions applied in both quasi-static and dynamic tests. Maintaining identical specimen geometry, indenter shape, and boundary conditions allows a direct comparison between the two loading methodologies. The primary difference lies in the loading rate and control strategy, which governs inertia effects and strain rate sensitivity. This controlled comparison is essential for isolating the influence of variable dynamic loads on multiaxial stress and deformation behavior.

Table 3; Maximum Recorded Forces under Variable Loading Conditions

Test type	Average peak force (kN)	Standard deviation (%)
QSI	4.85	6.2
LVI	5.43	9.8

As shown in Table 3, the dynamic loading condition produces higher peak forces compared to quasi-static loading. This increase is attributed to inertia effects and rate-dependent stiffness enhancement. However, higher force levels do not necessarily imply earlier damage initiation, highlighting the importance of complementary energy-based and strain-based analyses in multiaxial loading studies.

Table 4; Critical Internal Energy Values at Key Damage Events

Damage stage	QSI energy (J)	LVI energy (J)	Difference (%)
Damage initiation	6.2	6.6	6.5
Damage propagation	11.8	12.1	3.0
Final failure	18.4	18.7	1.8

Table 4 demonstrates a strong correlation between quasi-static and dynamic tests when analyzed in terms of internal energy. Despite differences in force response, the critical energy levels associated with damage initiation and evolution remain remarkably similar. This confirms that internal energy is a robust parameter for predicting failure in mechanical structures subjected to variable dynamic loads.

Table 5; Maximum Principal Strain Levels at Critical Locations

Location	QSI max strain (%)	LVI max strain (%)
Plate centre (bottom surface)	0.82	0.86
Near indenter (top surface)	0.64	0.69
Plate edge	0.91	0.95

The strain values presented in Table 5 reveal comparable strain magnitudes under both loading regimes. Slightly higher strains observed in dynamic tests are associated with transient stress amplification. The highest tensile strains occur at the plate edges and bottom surface, consistent with bending-dominated multiaxial stress states and boundary-induced constraints.

Table 6; Comparison between Experimental and Numerical Strain Predictions

Analysis method	Maximum strain (%)	Error relative to experiment (%)
Experimental (DIC / strain gauges)	0.85	—
FEM prediction	0.81	4.7

Table 6 highlights the strong agreement between experimental measurements and finite element simulations. The small discrepancy confirms the capability of the numerical model to capture multiaxial stress interaction and deformation localization prior to damage initiation. This validates the use of FEM as a predictive tool for assessing structural behavior under variable dynamic loading. As a consequence of this flexural orthotropy, the strain gradients originating from the centre of the plate do not propagate uniformly along the geometric axes. Instead, they advance along directions close to the orthogonal axes but exhibit a slight deviation toward the direction associated with maximum stiffness. This behaviour reflects the dominant role of fibre orientation in governing strain redistribution under bending and contact loading. Furthermore, the influence of the circular support conditions becomes evident through the appearance of elevated tensile strain levels near the plate edges, where boundary-induced constraints interact with bending deformation to amplify local strain concentrations.

4. Conclusion

A comprehensive analysis of quasi-static indentation and low-velocity impact tests, instrumented for the measurement of strain states, applied forces, and accumulated internal energy throughout the loading process, has revealed a strong correlation between the structural responses obtained from both methodologies. Despite the pronounced differences in apparent stiffness associated with varying loading rates, the most significant transitions in mechanical behaviour consistently occur at comparable levels of internal energy.These findings indicate that damage initiation and subsequent evolution are primarily governed by energy- based criteria rather than by the applied strain rate. The critical stages of structural response, marked by changes in stiffness and deformation patterns, are observed under both testing approaches at similar internal energy thresholds. Moreover, the progressive nature of the quasi-static methodology provides enhanced insight into the sequence and interaction of failure mechanisms, facilitating a clearer interpretation of damage development that is otherwise more difficult to capture under dynamic loading conditions. Overall, the results support the use of quasi-static testing as a reliable and effective tool for investigating damage mechanisms in mechanical structures subjected to variable dynamic loads, particularly when the analysis is framed in terms of multiaxial stress states and internal energy evolution.

Ackowledgements

The author would like to express sincere appreciation to the University of Dijlah for the academic support and facilities provided, which contributed significantly to the completion of this research. The author also extends gratitude to all those who assisted in the successful accomplishment of this work.

References

[1] Abrate, S. Impact on Composite Structures. Cambridge University Press, Cambridge, UK, 1998.
[2] Abrate, S. Modelling of Impacts on Composite Structures. Composite Structures 2001, 51, 129–138.
[3] Cantwell, W.J.; Morton, J. The Impact Resistance of Composite Materials—A Review. Composites 1991, 22, 347–362.
[4] Davies, G.A.O.; Hitchings, D.; Ankersen, J. Predicting Delamination and Debonding in Laminated Composite Structures Subjected to Low-Velocity Impact. Composites Science and Technology 2006, 66, 846–854.
[5] Hallett, S.R.; Jiang, W.G.; Khan, B.; Wisnom, M.R. Modelling the Interaction between Matrix Cracking and Delamination Damage in Composite Laminates. Composites Science and Technology 2008, 68, 80–89.
[6] Richardson, M.O.W.; Wisheart, M.J. Review of Low-Velocity Impact Properties of Composite Materials. Composites Part A: Applied Science and Manufacturing 1996, 27, 1123–1131.
[7] Iannucci, L.; Willows, M. An Energy-Based Damage Mechanics Approach to Modelling Impact onto Woven Composite Materials—Part I: Numerical Models. Composites Part A: Applied Science and Manufacturing 2006, 37, 2041–2056.

[8] Zhang, X.; Hounslow, L.; Grassi, M. Improvement of Low-Velocity Impact and Compression-After-Impact Performance by Z-Fibre Pinning. Composites Science and Technology 2008, 68, 3394–3403.
[9] Soutis, C. Fibre Reinforced Composites in Aircraft Construction. Progress in Aerospace Sciences 2005, 41, 143–151.
[10] Hou, J.P.; Petrinic, N.; Ruiz, C.; Hallett, S.R. Prediction of Impact Damage in Composite Plates. Composites Science and Technology 2000, 60, 273–281.
[11] Sun, C.T.; Chen, J.K. On the Impact of Laminated Composite Plates. Journal of Composite Materials 1989, 23, 478–492.
[12] Schuecker, C.; Pettermann, H.E. Identification of Damage Mechanisms in Composite Laminates Subjected to Indentation. Composites Part A: Applied Science and Manufacturing 2007, 38, 185–195.
[13] Lopes, C.S.; González, E.V.; Zenkert, D.; Camanho, P.P.; Gürdal, Z. Low-Velocity Impact Damage on Dispersed Stacking Sequence Laminates. Composites Science and Technology 2009, 69, 926–936.
[14] Feraboli, P.; Kedward, K.T. Enhanced Structural Modeling of Low-Velocity Impact on Composite Laminates. Journal of Composite Materials 2006, 40, 1943–1962.
[15] Belingardi, G.; Cavatorta, M.P.; Duella, R. Material Characterization of a Composite-Foam Sandwich for the Front Structure of a High-Speed Train. Composite Structures 2003, 61, 13–25.

Biographies of Authors

The recommended number of authors is at least 2. One of them as a corresponding author.
Please attach clear photo (3x4 cm) and vita. Example of biographies of authors:

Eng. Ali Alamara is an Iraqi engineer specializing in Health, Safety and Environment (HSE) and Lifting Planning and Supervision, with more than 15 years of professional experience in oil and gas, drilling, construction, and energy projects in Iraq. He has held various positions including HSE Manager, HSE Lead, HSE Supervisor, Lifting Planner, Lifting Supervisor, and Permit to Work (PTW) Coordinator, and has worked with local and international companies in cooperation with organizations such as LUKOIL, ENI, STX, HYUNDAI, and KUWAIT ENERGY.
He possesses extensive expertise in safety risk management, site inspections, incident investigation, critical lifting plans, permit-to-work systems, risk assessment, and emergency response planning, as well as supervising safety teams and delivering training programs. He holds several recognized professional certifications, including NEBOSH IGC, ISO 45001 Lead Implementer, OSHA, IOSH, Lifting Supervisor, Risk Assessment, Confined Space, Fire Fighting, and First Aid, in addition to certifications from OSHAcademy and Autodesk AutoCAD. He is fluent in Arabic and has excellent proficiency in English, with strong skills in AutoCAD and Microsoft Office.